Layer-skipping connections improve the effectiveness of equilibrium propagation on layered networks

Jimmy Gammell [1,*]**, Sonia M. Buckley** [1]**,Sae Woo Nam** [1] **and Adam N. McCaughan** [1]

[1]*National Institute of Standards and Technology, Boulder, CO, United States*

Correspondence*:
Jimmy Gammell
jimmy.gammell@colorado.edu

2 ABSTRACT

3 Equilibrium propagation is a learning framework that marks a step forward in the search for a
4 biologically-plausible implementation of deep learning, and could be implemented efficiently in
5 neuromorphic hardware. Previous applications of this framework to layered networks encountered
6 a vanishing gradient problem that has not yet been solved in a simple, biologically-plausible
7 way. In this paper, we demonstrate that the vanishing gradient problem can be mitigated by
8 replacing some of a layered network's connections with random layer-skipping connections in a
9 manner inspired by small-world networks. This approach would be convenient to implement in
10 neuromorphic hardware, and is biologically-plausible.

11 **Keywords: equilibrium propagation, deep learning, small-world, layer-skipping connections, neuromorphic computing, biologically-**
12 **motivated**

13 **Number of words: 3152**

14 **Number of figures: 7**

15 **Number of tables: 1**

1 INTRODUCTION

16 As research into neural networks grows, there has been increased interest in designing biologically-inspired
17 training algorithms, as they may offer insight into biological learning processes and also offer clues
18 towards developing energy-efficient neuromorphic systems [Wozniak et al., 2018; Crafton et al., 2019;
19 Ernoult et al., 2020; Bartunov et al., 2018; Lillicrap et al., 2014; Bengio et al., 2015]. The equilibrium
20 propagation learning framework developed Scellier and Bengio [2016] is one such algorithm. It is a
21 method for training a class of energy-based networks, the prototype for which is the continuous Hopfield
22 network Hopfield [1984]. In particular, it addresses one of the major issues that prevent other training
23 algorithms (such as backpropagation) from being biologically-plausible, which is the requirement for
24 separate computation pathways for different phases of training. This also makes the algorithm appealing for

25 practical implementation into neuromorphic hardware, because only a single computation circuit is required
26 within each (non-output) neuron, rather than multiple distinct circuits. However, current implementations
27 of the algorithm still have a defect that diminishes its biological plausibility: they require hand-tuned
28 per-layer hyperparameters to account for a vanishing gradient through the network. In addition to not
29 being biologically plausible, these multiplicative hyperparameters would be difficult to implement in a
30 neuromorphic hardware system with limited bit depth. In this work, we demonstrate that the vanishing
31 gradient problem can instead be addressed through topological means: by randomly replacing some of a
32 layered network's connections with layer-skipping connections, we can generate a network that trains each
33 layer more evenly and does not need per-layer hyperparameters. This solution is biologically-plausible and
34 would be easier to implement in a neuromorphic system; additionally, it entails hand-tuning only two new
35 hyperparameters (the number of layer-skipping connections and their initial weights), whereas the original
36 solution adds a new hyperparameter for each pair of layers in a network.

37 Implementation of equilibrium propagation in [Scellier and Bengio, 2016] was hindered by a vanishing
38 gradient problem whereby networks with as few as 3 hidden layers trained slowly on MNIST [LeCun and
39 Cortes, 1998] – a serious issue given that network depth is critical to performance on difficult datasets
40 [Simonyan and Zisserman, 2014; Srivastava et al., 2015b] and that convergence to a low error rate on
41 MNIST is a low bar to meet. The problem was overcome in [Scellier and Bengio, 2016] by independently
42 tuning a unique learning rate for each layer in the network. These learning rates were multiplicative factors
43 that proportionally scaled the signals communicated between layers.

44 In our work, we have modified the strictly-layered topology of the original implementation by adding
45 and removing connections to create a small-world-like network[Watts and Strogatz, 1998]. Through
46 this modification we have eliminated the per-layer hyperparameters without substantially degrading the
47 algorithm's performance – after 250 epochs the modified network produces .0117% training error (out
48 of 50,000 examples) and 2.55% test error (out of 10,000 examples) on MNIST using a network with
49 three hidden layers and no regularization term in its cost function. These error rates are comparable to
50 those of other biologically-motivated networks [Bartunov et al., 2018] and are approximately the same as
51 those of the layered network with unique, manually-tuned learning rates in [Scellier and Bengio, 2016].
52 Our method could be implemented with relative ease in any system with configurable connectivity, such
53 as those already described in several neuromorphic hardware platforms [Davies et al., 2018; Schemmel
54 et al., 2010; Shainline et al., 2019]. Layer-skipping connections have been observed in biological brains
55 [Bullmore and Sporns, 2009], so the approach is biologically-plausible. Similar techniques have seen
56 success in convolutional [He et al., 2015; Srivastava et al., 2015a] and multilayer feedforward [Xiaohu
57 et al., 2011; Krishnan et al., 2019] networks. Our findings outlined in this paper suggest that layer-skipping
58 connections are effective-enough to be appealing in contexts where simplicity and biological plausibility
59 are important. While small-world networks are not a novel concept, to our knowledge our work is the first
60 to train small-world-like networks using the Equilibrium Propagation learning framework.

2 BACKGROUND

2.1 Equilibrium propagation

62 Similarly to backpropagation, the equilibrium propagation algorithm [Scellier and Bengio, 2016] trains
63 networks by approximating gradient descent on a cost function. Equilibrium propagation is applicable to
64 any network with dynamics characterized by evolution to a fixed point of an associated energy function;
65 our implementation is a recreation of that in [Scellier and Bengio, 2016], which applies it to a continuous

66 Hopfield network [Hopfield, 1984]. The mathematical formulation of the framework can be found in
67 [Scellier and Bengio, 2016]. We discuss its appeal over backpropagation in section A.

68 ### 2.1.1 Implementation in a continuous Hopfield network

69 Here we summarize the equations through which a continuous Hopfield network is trained using equili-
70 brium propagation; this summary is based on the more-thorough and more-general treatment in [Scellier
71 and Bengio, 2016].

72 Consider a network with n neurons organized into an input layer with p neurons, hidden layers with q
73 neurons and an output layer with r neurons. Let the activations of these neurons be denoted respectively
74 by vectors $\boldsymbol{x} \in \mathbb{R}^p$, $\boldsymbol{h} \in \mathbb{R}^q$ and $\boldsymbol{y} \in \mathbb{R}^r$, and let $\boldsymbol{s} = (\boldsymbol{h}^T, \boldsymbol{y}^T)^T \in \mathbb{R}^{q+r}$ and $\boldsymbol{u} = (\boldsymbol{x}^T, \boldsymbol{s}^T)^T \in \mathbb{R}^n$ be
75 vectors of, respectively, the activations of non-fixed (non-input) neurons and of all neurons in the network.
76 Let $\boldsymbol{W} \in \mathbb{R}^{n \times n}$ and $\boldsymbol{b} \in \mathbb{R}^n$ denote the network's weights and biases where w_{ij} is the connection weight
77 between neurons i and j and b_i is the bias for neuron i ($\forall i \; w_{ii} = 0$ to prevent self-connections), and let ρ
78 denote its activation function; here and in [Scellier and Bengio, 2016],

$$\rho(x) = \begin{cases} 0 & x < 0 \\ x & 0 \leq x \leq 1 \\ 1 & x > 1 \end{cases} \tag{1}$$

79 is a hard sigmoid function where $\rho'(0) = \rho'(1)$ is defined to be 1 to avoid neuron saturation. Let
80 $\boldsymbol{\rho}((x_1, \ldots, x_n)^T) = (\rho(x_1), \ldots, \rho(x_n))^T$.

81 The behavior of the network is to perform gradient descent on a total energy function F that is modified
82 by a training example $(\boldsymbol{x}_d, \boldsymbol{y}_d)$. Consider energy function $E : \mathbb{R}^n \to \mathbb{R}$,

$$E(\boldsymbol{u}; \boldsymbol{W}, \boldsymbol{b}) = \frac{1}{2}\boldsymbol{u}^T\boldsymbol{u} - \frac{1}{2}\boldsymbol{\rho}(\boldsymbol{u})^T \boldsymbol{W} \boldsymbol{\rho}(\boldsymbol{u}) - \boldsymbol{b}^T\boldsymbol{u} \tag{2}$$

83 and arbitrary cost function $C : \mathbb{R}^r \to \mathbb{R}_+$; here and in [Scellier and Bengio, 2016] it is a quadratic cost
84 function given by

$$C(\boldsymbol{y}) = \frac{1}{2}||\boldsymbol{y} - \boldsymbol{y}_d||_2^2, \tag{3}$$

85 though the framework still works for cost functions incorporating a regularization term dependent on $\boldsymbol{W}$
86 and $\boldsymbol{b}$. The total energy function $F : \mathbb{R}^n \to \mathbb{R}$ is given by

$$F(\boldsymbol{u}; \beta, \boldsymbol{W}, \boldsymbol{b}) = E(\boldsymbol{u}; \boldsymbol{W}, \boldsymbol{b}) + \beta C(\boldsymbol{y}) \tag{4}$$

87 where the clamping factor β is a small constant. $\boldsymbol{s}$ evolves over time t as

$$\frac{d\boldsymbol{s}}{dt} \propto -\frac{\partial F}{\partial \boldsymbol{s}}. \tag{5}$$

88 Equilibrium has been reached when $\frac{\partial F}{\partial \boldsymbol{s}} \approx 0$. This can be viewed as solving the optimization problem

$$\underset{\boldsymbol{s} \in \mathbb{R}^{q+r}}{\text{minimize}} F((\boldsymbol{x}_d^T, \boldsymbol{s}^T)^T; \beta, \boldsymbol{W}, \boldsymbol{b}) \tag{6}$$

89 by using gradient descent to find a local minimum of F.

90 The procedure for training on a single input-output pair $(\boldsymbol{x}_d, \boldsymbol{y}_d)$ is as follows:

91   1. Clamp $\boldsymbol{x}$ to $\boldsymbol{x}_d$ and perform the free-phase evolution: evolve to equilibrium on the energy function
92   $F(\boldsymbol{u}; 0, \boldsymbol{W}, \boldsymbol{b})$ in a manner dictated by equation 5. Record the equilibrium state $\boldsymbol{u}^0$.

93   2. Perform the weakly-clamped evolution: evolve to equilibrium on the energy function $F(\boldsymbol{u}; \beta, \boldsymbol{W}, \boldsymbol{b})$
94   using $\boldsymbol{u}^0$ as a starting point. Record the equilibrium state $\boldsymbol{u}^\beta$.

95   3. Compute the correction to each weight in the network:

$$\Delta W_{ij} = \frac{1}{\beta}(\rho(u_i^\beta)\rho(u_j^\beta) - \rho(u_i^0)\rho(u_j^0)). \tag{7}$$

96   Adjust the weights using $W_{ij} \leftarrow W_{ij} + \alpha \Delta W_{ij}$ where the learning rate α is a positive constant.

97   4. Compute the correction to each bias in the network:

$$\Delta b_i = \frac{1}{\beta}(\rho(u_i^\beta) - \rho(u_i^0)) \tag{8}$$

98   and adjust the biases using $b_i \leftarrow b_i + \alpha \Delta b_i$.

99   This can be repeated on as many training examples as desired. Training can be done on batches by
100 computing ΔW_{ij} and Δb_i for each input-output pair in the batch, and correcting using the averages of
101 these values. Note that the correction to a weight is computed using only the activations of neurons it
102 directly affects, and the correction to a bias is computed using only the activation of the neuron it directly
103 affects. This contrasts with backpropagation, where to correct a weight or bias l layers from the output it is
104 necessary to know the activations, derivatives and weights of all neurons between 0 and $l-1$ layers from
105 the output.

2.2   Vanishing gradient problem

107 Vanishing gradients are problematic because they reduce a network's rate of training and could be
108 difficult to represent in neuromorphic analog hardware due to limited bit depth. As a simple example, the
109 multiplicative factor of 0.008 used in previous implementations would lead to significant precision errors
110 in a system with signals represented by integers from 0-16 (bit depth of 4).

111 The vanishing gradient problem is familiar in the context of conventional feedforward networks, where
112 techniques such as the weight initialization scheme in [Glorot and Bengio, 2010], the use of activation
113 functions with derivatives that do not lead to output saturation [Schmidhuber, 2015], and batch norma-
114 lization [Ioffe and Szegedy, 2015] have been effective at overcoming it. However, in the context of the
115 networks trained in [Scellier and Bengio, 2016], the vanishing gradient problem persists even when the
116 former two techniques are used. To our knowledge batch normalization has not been used in the context of
117 equilibrium propagation; however, it seems unlikely to be biologically-plausible.

2.3   Related work

119 References [Lee et al., 2015; Xie and Seung, 2003; Pineda, 1987] describe other approaches to locally
120 approximating the gradient of a cost function. References [Lillicrap et al., 2014; Crafton et al., 2019]
121 explore the use of a random feedback matrix for backwards connections that is more biologically-plausible
122 than identical forwards and backwards connections. Reference [Bartunov et al., 2018] explores the present
123 state of biologically-motivated deep learning, and [Bengio et al., 2015] discusses the criteria a biologically-
124 plausible network would need to satisfy. References [Shainline et al., 2019; Davies et al., 2018; Nahmias
125 et al., 2013] discuss analog hardware that could potentially implement equilibrium propagation. References
126 [He et al., 2015; Srivastava et al., 2015a; Xiaohu et al., 2011; Krishnan et al., 2019] use layer-skipping

127 connections for other types of networks and learning frameworks. References [Ioffe and Szegedy, 2015;
128 Glorot and Bengio, 2010] give approaches to solving vanishing gradient problems.

3 IMPLEMENTATION

We implemented [1] the Equilibrium Propagation framework described in [Scellier and Bengio, 2016] using
Pytorch [Paszke et al., 2019]. Like the networks in [Scellier and Bengio, 2016], our networks are continuous
Hopfield networks with a hard sigmoid activation function

$$\sigma(x) = \text{Max}\{0, \text{Min}\{x, 1\}\}$$

and squared-error cost function with no regularization term

$$C = ||\boldsymbol{y} - \boldsymbol{y}_d||_2^2,$$

129 where $\boldsymbol{y}$ is the network's output and $\boldsymbol{y}_d$ is the target output.

130   We use two performance-enhancing techniques that were used in [Scellier and Bengio, 2016]: we
131 randomize the sign of β before training on each batch, which was found in the original paper to have a
132 regularization effect, and we use persistent particles, where the state of the network after training on a
133 given batch during epoch n is used as the initial state for that batch during epoch $n + 1$. Persistent particles
134 reduce the computational resources needed to approximate the differential equation governing network
135 evolution, and would be unnecessary in an analog implementation that can approximate the equation
136 efficiently. Note that this technique leads to higher error rates early in training than would be present with a
137 more-thorough approximation of the differential equation. For purposes of computational efficiency we
138 compute training error throughout training by recording the classification error on each training batch
139 prior to correcting the network's parameters, and we compute the test error by evolving to equilibrium
140 and evaluating classification error for each batch in the test dataset after each full epoch of training. In
141 some of our trials (e.g. figure 4) this approach causes the training error to exceed the test error early on in
142 training because the network has undergone only part of an epoch of training prior to evaluating error on
143 each training batch, but a full epoch prior to evaluating error on each test batch.

144   In all networks we use the weight initialization scheme in [Glorot and Bengio, 2010] for the weights
145 of interlayer connections; weights connecting a pair of layers with n_1 and n_2 neurons are taken from the
146 uniform distribution $U[-\sqrt{\frac{6}{n_1+n_2}}, \sqrt{\frac{6}{n_1+n_2}}]$. We have found empirically that for new connections added
147 in our topology, for a network with N layers it works reasonably well to draw all initial weights from
148 $U[-a, a]$ where $a = \frac{1}{N} \sum_{i=1}^{N-1} \sqrt{\frac{6}{n_i+n_{i+1}}}$ and n_i denotes the number of neurons in layer i.

3.1 Multilayer feedforward (MLFF) topology

150   The purpose of this paper is to address the vanishing gradient problem that is present in networks with a
151 multilayer feedforward (MLFF) topology in [Scellier and Bengio, 2016]. Therefore, we have done a variety
152 of trials on networks with MLFF topology to provide points of reference. The MLFF topology is illustrated
153 to the left in figure 1; it consists of layers of neurons with connections between every pair of neurons in
154 adjacent layers, no connections within layers, and no connections between neurons in non-adjacent layers.

155   In some trials we use a single global learning rate α, and in other trials we use per-layer rates individually
156 tuned to counter the vanishing gradient problem. The latter case entails $N + 1$ unique learning rates

---

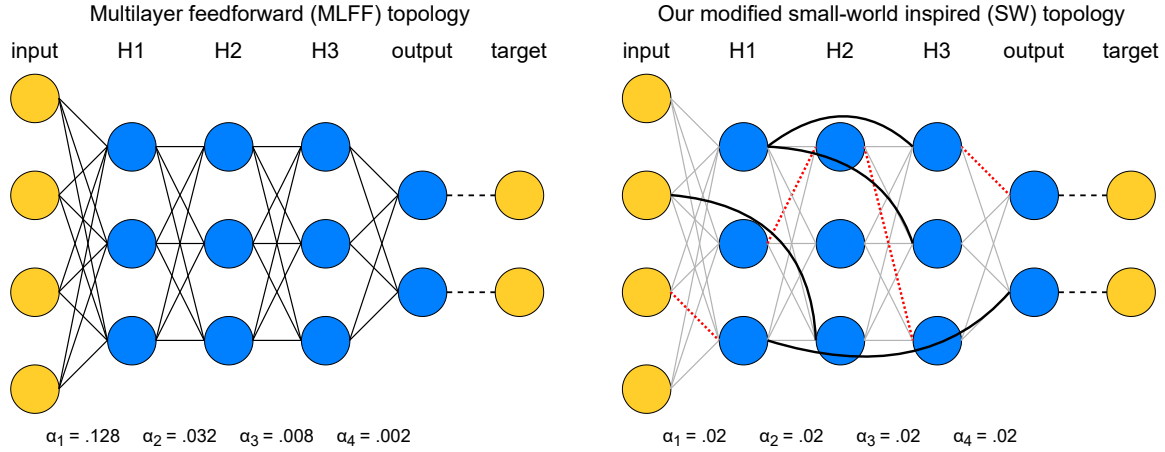[1] https://github.com/jgammell/Equilibrium_Propagation_mobile.git

Figure 1. Illustration of our topological modifications to mitigate the vanishing gradient problem while using a global learning rate. (left) A network with MLFF topology as tested in [Scellier and Bengio, 2016]. Observe that the learning rate increases by a factor of 4 each time the distance from the output increases by one layer. (right) A network with SW topology, where a subset of connections have been replaced by random layer-skipping connections and per-layer learning rates have been replaced by a single global learning rate. Red dotted lines denote removed connections and solid black lines denote the layer-skipping connections replacing them.

157 $\alpha_i, \ i = 1, \ldots, N + 1$ for a network with N hidden layers, where the weights connecting layers i and $i + 1$
158 and the biases in layer i have learning rate α_i.

3.2 Small-world inspired (SW) topology

Algorithm 1: Algorithm to generate SW topology starting with a network with MLFF topology

Input: Network with MLFF topology to modify
Parameter: Probability p with which to replace a given preexisting connection
Output: Modified network with SW topology

network $\leftarrow$ input network with MLFF topology
potentialConns $\leftarrow$ {pairs of distinct neurons in distinct layers that do not share a connection}

for existing connection ec in network **do**
    pp $\leftarrow$ value drawn from uniform distribution $U[0, 1]$
    if pp $< $ p **then**
        remove connection ec in network
        randomly draw connection pc from potentialConns
        make connection pc in network
        remove pc from potentialConns
        add ec to potentialConns

---

160 We generate a network with small-world inspired (SW) topology by first starting with a MLFF topology
161 as described above in section 3.1, then applying an algorithm similar to the one described in [Watts and
162 Strogatz, 1998] to randomly replace [2] existing connections by random layer-skipping connections with
163 some probability p. This is done using algorithm 1, and the resulting SW topology is illustrated to the right
164 in figure 1. In all of our trials networks with SW topology are trained using a single global learning rate α.

---

[2] We have done a small number of trials in which layer skipping connections are added without removing an equal number of preexisting connections, and have observed behavior similar to that resulting from using algorithm 1.
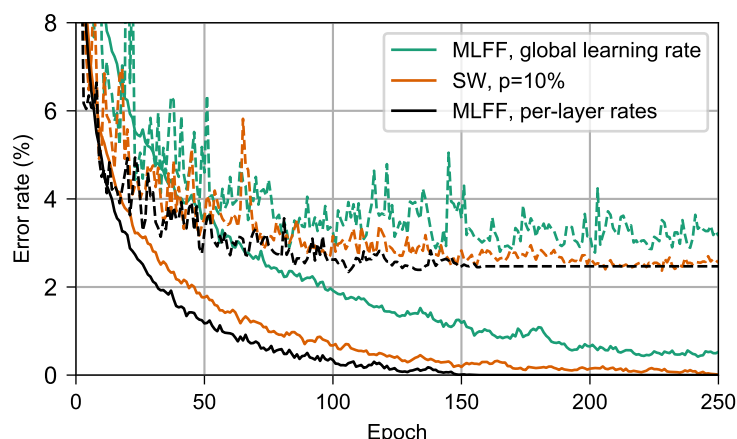

Figure 2. Performance on MNIST of networks with 3 500-neuron hidden layers. Dashed lines show the test error and solid lines show the training error. In black is a MLFF network with per-layer rates individually tuned to counter the vanishing gradient problem. In green is the same MLFF network but with a single global learning rate. In orange is a network with SW topology, $p = 10\%$. Observe that the network with our topology trains almost as quickly as a network with per-layer rates, and significantly more-quickly than a network with a single learning rate.

4 RESULTS

4.1 Evaluation on MNIST dataset

Here we compare the behavior of networks with the SW topology presented here to those with the MLFF topology used in [Scellier and Bengio, 2016] when training on the MNIST dataset. We are using this dataset because it allows us to reproduce and extend the trials in [Scellier and Bengio, 2016], and because it is non-trivial to effectively train on yet small enough to allow trials to complete in a reasonably-short amount of time.

4.1.1 Classification error

Figure 2 shows the results of comparing the classification error on MNIST of a network with SW topology to that of a MLFF network with individually-tuned per-layer learning rates, as in [Scellier and Bengio, 2016], and to that of a MLFF network with a single global learning rate. For all networks we use 3 500-neuron hidden layers, $\epsilon = .5$, $\beta = 1.0$, 500 free-phase iterations, 8 weakly-clamped-phase iterations, and train for 250 epochs. For the SW network we use $p = 10\%$ and a global learning rate $\alpha = .02$. For the MLFF network with per-layer rates we use learning rates $\alpha_1 = .128$, $\alpha_2 = .032$, $\alpha_3 = .008$ and $\alpha_4 = .002$. For the MLFF network with a single global learning rate, we use learning rate $\alpha = .02$.

We find that both the SW network and the MLFF network with per-layer rates significantly outperform the MLFF network with a single global learning rate during the first 250 epochs of training. The SW network achieves training and test error rates similar to those of the MLFF network with per-layer rates, albeit after around 100 additional epochs of training.

4.1.2 Training rates of individual pairs of layers

Here we consider the first 100 epochs of the trials described in section 4.1.1 above and track the root-mean-square correction to weights connecting each pair of adjacent layers. Figure 3 shows these values for the 3 network topologies, recorded after each batch and averaged over each epoch.

We can clearly see the vanishing gradient problem for the MLFF network with a single global learning rate (left), manifesting as attenuation with depth of the root-mean-square corrections to weights. The
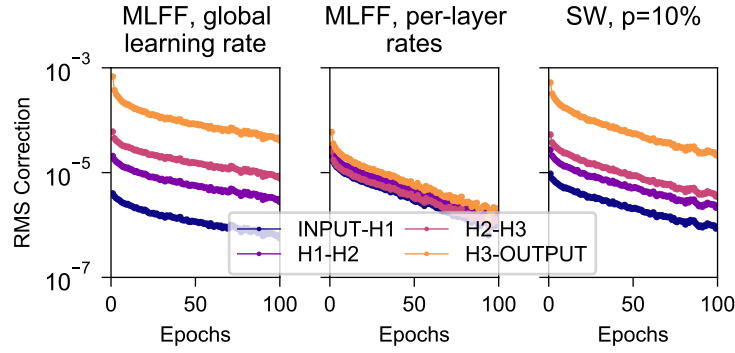
Figure 3. Root mean square corrections to weights in different layers while training on MNIST, for networks with 3 500-neuron hidden layers. Measurements were taken after each batch, and averaged over each epoch. (left) A MLFF network with a single global learning rate. (center) A MLFF network with per-layer rates individually tuned to counter the vanishing gradient problem. (right) A network with SW topology, $p = 10\%$. Observe that the correction magnitudes attenuate significantly with depth in the MLFF network with a single global learning rate, and that a network with SW topology reduces the severity of the issue, albeit less-effectively than individually tuning a learning rate for each layer.

189 problem is addressed very-effectively by the use of manually-tuned per-layer learning rates (center), and is
190 mitigated to a more-modest extent when we use SW topology with a global learning rate. It is noteworthy
191 that the speed of training of these networks as shown in figure 2 is commensurate with the uniformity with
192 which their layers train as shown in figure 3.

193   It can be seen that in the network with SW topology the weights connecting to the output layer train
194 significantly faster than deeper weights, which cluster together; we have observed similar behavior in
195 a variety of datasets and network dimensions. We suspect it has to do with the fact that output neurons
196 connect directly to the target output, whereas because layer-skipping connections are not attached to the
197 target output the other layers must connect indirectly through at least 2 connections.

198 4.1.3   Behavior for varying p

199   Figure 4 shows the behavior during the first 10 epochs of training on MNIST for a network with SW
200 topology as p is increased from 0 to .727. The network being tested has 5 100-neuron hidden layers and is
201 trained with learning rate $\alpha = .015$, $\epsilon = .5$, $\beta = 1.0$, 500 free-phase iterations and 8 weakly-clamped-phase
202 iterations.

203   We see in the top graph that the training and test error rates after 10 epochs decay exponentially as p
204 increases. The bottom graph indicates that the RMS corrections to weights become more-uniform with
205 depth as p increases. Corrections to layers that do not connect directly to the output layer cluster closer
206 together as p increases, but it appears that the corrections to weights connecting directly to the output layer
207 train faster than deeper weights with a gap that does not appear to decrease with p; this is similar to the
208 behavior seen in section 4.1.2.

209   To quantify the spread of the RMS corrections as a single scalar, we introduce the statistic

$$\text{log-spread} = \text{Std. dev}\{\log_{10}(w_l), l = 1, \dots, N + 1\} \tag{9}$$

210 where N denotes the number of hidden layers in a network and w_l denotes the root mean square magnitude
211 of corrections to weights connecting the lth and $l + 1^{th}$ layers from the input, averaged over all epochs of
212 training. The log-spread is plotted in the top graph alongside the error rate, and these values can be seen to
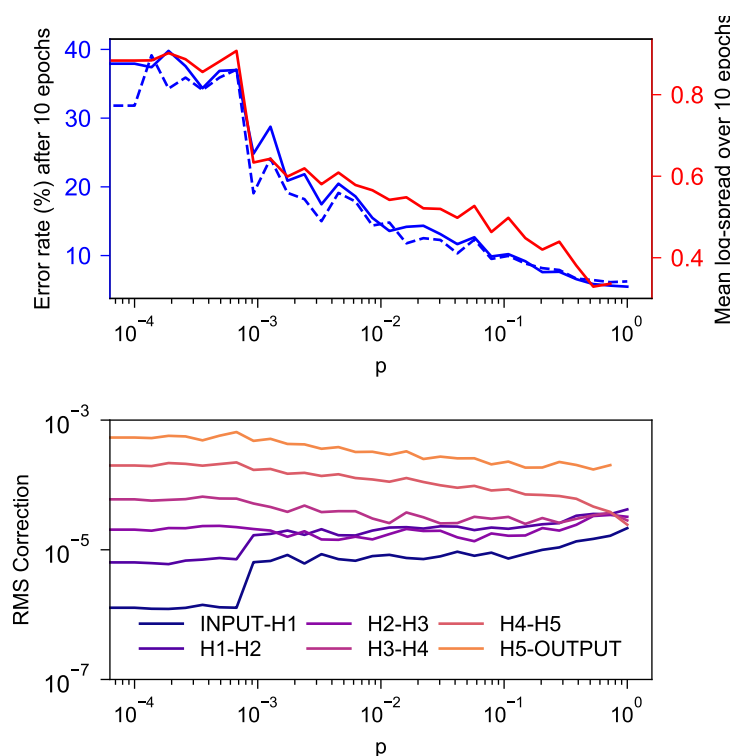

Figure 4. Behavior during the first 10 epochs of training on MNIST for a SW network with 5 100-neuron hidden layers for various values of p. (top) In solid and dashed blue are the training and test error rates after 10 epochs and in red is the log-spread (equation 9) averaged over the 10 epochs. As expected, both values decrease as p increases. There appears to be a strong linear correlation between the two, with coefficient of determination $r^2 = .970$. This is consistent with our suspicion that mitigation of the vanishing gradient problem is the reason our topology tends to increase the rate at which layered networks train. (bottom) Root mean square corrections to weights in different layers, averaged over the 10 epochs. As expected, the spread of these values decreases as p increases.

213   have a strong linear correlation. The training error and the log-spread have a coefficient of determination
214    $r^2 = .970$.

215   ### 4.1.4   Weight correction matrix

216   In figure 5 we visualize the mean weight correction matrices resulting from training a MLFF network and
217   a SW network with 5 100-neuron hidden layers as described in section 4.1.3. Training on a batch yields a
218   correction matrix $\mathbf{dW}$ where element $\mathbf{dW}_{ij}$ denotes the change to the connection weight between neurons
219   i and j; here we have recorded a matrix with element (i, j) containing the average of $|\mathbf{dW}_{ij}|$ over 100
220   epochs of training and displayed it as an image with the color of a pixel at position (i, j) encoding the
221   magnitude of $|\mathbf{dW}_{ij}|$ as indicated by the legend.

222   As expected, there is attenuation with depth to weight correction magnitudes in a MLFF network with a
223   single global learning rate, and transitioning to a network with SW topology reduces the severity of the
224   problem. An interesting feature of the SW matrix that is visible upon close inspection is that layer-skipping
225   connections tend to receive larger correction magnitudes when they are closer to the output of the network.
226   Striations can be seen in correction magnitudes, which we believe correspond to sections of images in the
227   MNIST dataset that contain varying amounts of information; for example, for corrections connecting to the
228   input layer, there are 28 striations which likely correspond to the 28 rows of pixels in an image of a digit,
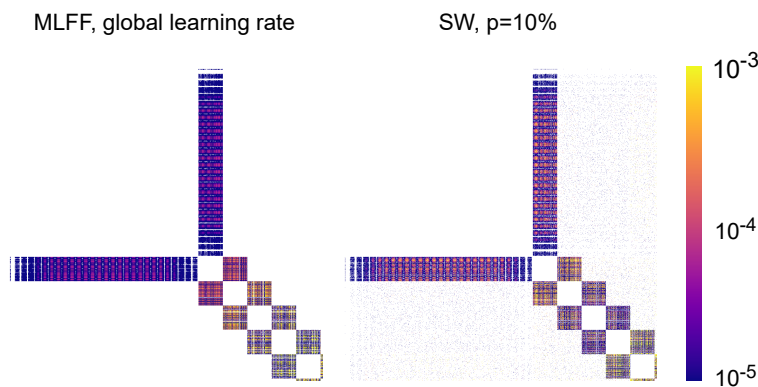
Figure 5. Mean absolute value correction matrix over 100 epochs for networks with 5 100-neuron hidden layers. A pixel at position (i, j) corresponds to the magnitude of the correction to the connection weight between neurons i and j. (left) A network with MLFF topology and a single global learning rate. (right) A network with SW topology, $p = 10\%$. Observe that attenuation of these values with depth is less-significant in the latter than in the former.

229 with pixels closer to the edges of the images typically blank and pixels closer to the centers of the images
230 typically containing most of the variation that encodes a digit.

231 ## 4.2 Evaluation on various datasets and topologies

232 Here we evaluate the presence of the vanishing gradient problem and the effectiveness of our topology at
233 addressing it on MNIST [LeCun and Cortes, 1998], Fashion MNIST (FMNIST) [Xiao et al., 2017], and
234 the diabetes and wine toy datasets distributed in scikit-learn [Pedregosa et al., 2011] with various network
235 architectures. Our results are shown in table 1. For all of these trials we use $\beta = 1.0$ and $\epsilon = .5$. While
236 hyperparameters in these trials have not been thoroughly optimized, the trials serve to illustrate that the
237 trends we saw on the MNIST dataset in section 4.1 hold for deeper networks and for networks training on
238 4 different datasets.

239 We report the training and test error after 100 epochs, as well as the log-spread (equation 9). We see that
240 networks with SW topology, $p = 10\%$, have a consistently smaller log-spread than networks with a MLFF
241 topology and a single global learning rate. Here this associated with smaller training and test error rates,
242 though we have seen for some less-optimized combinations of hyperparameters that the error rates do not
243 significantly change. We have observed that all of these networks behave in ways that are qualitatively
244 similar to the networks explored in section 4.1.

5 DIRECTIONS FOR FUTURE RESEARCH

245 There are several directions in which future research could be taken:

246 • Evaluating the effectiveness of this approach on hard datasets, such as CIFAR and ImageNet.

247 • Evaluating the effect of p on a network's test error in the long term.

248 • Exploring the effectiveness of a network when layer-skipping connections are used during training and
249 removed afterwards.

250 • Devise and mathematically justify a weight initialization scheme for layer-skipping connections.

251 • Mathematically justify the empirical results we have seen when using SW topology.

Dataset	Layer sizes	Topology	L.R.	Iterations	Error (train/test)	log-spread
Diabetes	10-10-10-10-10-10-1	MLFF	.01	1000/12	.0326/.0441	1.085
Diabetes	10-10-10-10-10-10-1	SW, p=10%	.01	1000/12	.0302/.0394	**.557**
Diabetes	10-10-10-10-10-10-10-10-10-1	MLFF	.01	5000/18	.0318/.0425	2.490
Diabetes	10-10-10-10-10-10-10-10-10-1	SW, p=10%	.01	5000/18	.0230/.0339	**.442**
Wine	13-10-10-10-10-10-3	MLFF	.01	1000/12	.680/.760	1.216
Wine	13-10-10-10-10-10-3	SW, p=10%	.01	1000/12	.467/.280	**.689**
Wine	13-10-10-10-10-10-10-10-3	MLFF	.01	5000/18	.653/.720	1.734
Wine	13-10-10-10-10-10-10-10-3	SW, p=10%	.01	5000/19	.253/.560	**.471**
MNIST	784-500-500-500-10	MLFF	.02	500/8	.0170/.0310	.689
MNIST	784-500-500-500-10	SW, p=10%	.02	500/8	.00675/.0272	**.545**
MNIST	784-100-100-100-100-100-10	MLFF	.015	1000/12	.156/.131	.867
MNIST	784-100-100-100-100-100-10	SW, p=10%	.015	1000/12	.0407/.0540	**.450**
FMNIST	784-100-100-100-100-100-10	MLFF	.015	1000/12	.266/.255	.862
FMNIST	784-100-100-100-100-100-10	SW, p=10%	.015	1000/12	.152/.164	**.484**

Table 1. Comparison of MLFF and SW topologies with various datasets and network architectures. Trials were run for 100 epochs with batch size 20 on MNIST and FMNIST and for 10 epochs with batch size 5 on Diabetes and Wine. Observe that the vanishing gradient problem, quantified by the log-spread (equation 9), is consistently less-severe when using the SW topology over the MLFF topology. Error is given as proportion of classes incorrectly identified for MNIST, FMNIST and Wine (classification problems) and as mean absolute value of error for Diabetes (regression problem).

CONFLICT OF INTEREST STATEMENT

252 The authors declare that the research was conducted in the absence of any commercial or financial
253 relationships that could be construed as a potential conflict of interest.

254   The U.S. Government is authorized to reproduce and distribute reprints for governmental purposes
255 notwithstanding any copyright annotation thereon.

REFERENCES

256 Bartunov, S., Santoro, A., Richards, B. A., Hinton, G. E., and Lillicrap, T. P. (2018). Assessing the
257   scalability of biologically-motivated deep learning algorithms and architectures. *CoRR* abs/1807.04587
258 Bengio, Y., Lee, D., Bornschein, J., and Lin, Z. (2015). Towards biologically plausible deep learning.
259   *CoRR* abs/1502.04156
260 Bullmore, E. and Sporns, O. (2009). Complex brain networks: graph theoretical analysis of structural and
261   functional systems. *Nature*
262 Crafton, B., Parihar, A., Gebhardt, E., and Raychowdhury, A. (2019). Direct feedback alignment with
263   sparse connections for local learning. *CoRR* abs/1903.02083
264 Davies, M., Srinivasa, N., Lin, T.-H., Chinya, G., Joshi, P., Lines, A., et al. (2018). Loihi: A neuromorphic
265   manycore processor with on-chip learning. *IEEE Micro* PP, 1–1. doi:10.1109/MM.2018.112130359
266 Ernoult, M., Grollier, J., Querlioz, D., Bengio, Y., and Scellier, B. (2020). Equilibrium propagation with
267   continual weight updates
268 Glorot, X. and Bengio, Y. (2010). Understanding the difficulty of training deep feedforward neural
269   networks. In *Proceedings of the Thirteenth International Conference on Artificial Intelligence and*

270 *Statistics*, eds. Y. W. Teh and M. Titterington (Chia Laguna Resort, Sardinia, Italy: PMLR), vol. 9 of
271 *Proceedings of Machine Learning Research*, 249–256

272 He, K., Zhang, X., Ren, S., and Sun, J. (2015). Deep residual learning for image recognition. *CoRR*
273 abs/1512.03385

274 Hopfield, J. (1984). Neurons with graded response have collective computational properties like those of
275 two-state neurons. *Proceedings of the National Academy of Sciences of the United States of America* 81,
276 3088–92. doi:10.1073/pnas.81.10.3088

277 Indiveri, G., Linares-Barranco, B., Hamilton, T., van Schaik, A., Etienne-Cummings, R., Delbruck, T., et al.
278 (2011). Neuromorphic silicon neuron circuits. *Frontiers in Neuroscience* 5, 73. doi:10.3389/fnins.2011.
279 00073

280 Ioffe, S. and Szegedy, C. (2015). Batch normalization: Accelerating deep network training by reducing
281 internal covariate shift. *CoRR* abs/1502.03167

282 Krishnan, G., Du, X., and Cao, Y. (2019). Structural pruning in deep neural networks: A small-world
283 approach

284 [Dataset] LeCun, Y. and Cortes, C. (1998). The mnist database of handwritten digits

285 Lee, D.-H., Zhang, S., Fischer, A., and Bengio, Y. (2015). Difference target propagation. 498–515.
286 doi:10.1007/978-3-319-23528-8_31

287 Lillicrap, T. P., Cownden, D., Tweed, D. B., and Akerman, C. J. (2014). Random feedback weights support
288 learning in deep neural networks

289 Nahmias, M., Shastri, B., Tait, A., and Prucnal, P. (2013). A leaky integrate-and-fire laser neuron for
290 ultrafast cognitive computing. *Selected Topics in Quantum Electronics, IEEE Journal of* 19, 1–12.
291 doi:10.1109/JSTQE.2013.2257700

292 Paszke, A., Gross, S., Massa, F., Lerer, A., Bradbury, J., Chanan, G., et al. (2019). Pytorch: An imperative
293 style, high-performance deep learning library. In *Advances in Neural Information Processing Systems*
294 *32*, eds. H. Wallach, H. Larochelle, A. Beygelzimer, F. d'Alché-Buc, E. Fox, and R. Garnett (Curran
295 Associates, Inc.). 8024–8035

296 Pedregosa, F., Varoquaux, G., Gramfort, A., Michel, V., Thirion, B., Grisel, O., et al. (2011). Scikit-learn:
297 Machine learning in Python. *Journal of Machine Learning Research* 12, 2825–2830

298 Pineda, F. (1987). Generalization of back-propagation to recurrent neural networks. *Physical Review*
299 *Letters* 59, 2229–2232

300 Scellier, B. and Bengio, Y. (2016). Equilibrium propagation: Bridging the gap between energy-based
301 models and backpropagation

302 Schemmel, J., Brüderle, D., Grübl, A., Hock, M., Meier, K., and Millner, S. (2010). A wafer-scale
303 neuromorphic hardware system for large-scale neural modeling. *Proceedings of 2010 IEEE International*
304 *Symposium on Circuits and Systems* , 1947–1950

305 Schmidhuber, J. (2015). Deep learning in neural networks: An overview. *Neural Networks* 61, 85–117.
306 doi:10.1016/j.neunet.2014.09.003

307 Shainline, J. M., Buckley, S. M., McCaughan, A. N., Chiles, J. T., Jafari Salim, A., Castellanos-Beltran,
308 M., et al. (2019). Superconducting optoelectronic loop neurons. *Journal of Applied Physics* 126, 044902.
309 doi:10.1063/1.5096403

310 Simonyan, K. and Zisserman, A. (2014). Very deep convolutional networks for large-scale image
311 recognition

312 Srivastava, R. K., Greff, K., and Schmidhuber, J. (2015a). Highway networks. *CoRR* abs/1505.00387

313 Srivastava, R. K., Greff, K., and Schmidhuber, J. (2015b). Training very deep networks

314 Watts, D. and Strogatz, S. (1998). Collective dynamics of 'small-world' networks. *Nature*

315 Wozniak, S., Pantazi, A., and Eleftheriou, E. (2018). Deep networks incorporating spiking neural dynamics.
316   *CoRR* abs/1812.07040
317 [Dataset] Xiao, H., Rasul, K., and Vollgraf, R. (2017). Fashion-mnist: a novel image dataset for
318   benchmarking machine learning algorithms
319 Xiaohu, L., Xiaoling, L., Jinhua, Z., Yulin, Z., and Maolin, L. (2011). A new multilayer feedforward small-
320   world neural network with its performances on function approximation. In *2011 IEEE International
321   Conference on Computer Science and Automation Engineering*
322 Xie, X. and Seung, H. (2003). Equivalence of backpropagation and contrastive hebbian learning in a
323   layered network. *Neural computation* 15, 441–54. doi:10.1162/089976603762552988

TABLES

	Backpropagation	Equilibrium Propagation
Number of distinct computations	2 – computations during forwards and backwards phases are distinct	≈ 1 – hidden neurons perform same computation in both phases. Output neurons perform a similar but modified version of the same computation.
Types of connections	Unidirectional to transmit activation to shallower neighbors and error to deeper neighbors	Bidirectional to each neighbor
Memory	Space to store activation and error term for each neuron	Space to store free and weakly-clamped activations for each neuron
Order of computations	Forwards propagation phase where layers are computed from deepest to shallowest; backwards propagation phase where layers are computed from shallowest to deepest; parameter update phase	Free phase where all neurons evolve simultaneously; weakly-clamped phase where all neurons evolve simultaneously; parameter update phase
Nonlinear activation function	Yes	Yes
Derivative of nonlinear activation function	Yes	Yes
Correction computation	Corrections require dedicated circuitry unique from that implementing propagation	Corrections require dedicated circuitry unique from that implementing evolution

Table 2. Comparison of the capabilities a hardware neuron would need in order to implement backpropagation and equilibrium propagation.

A COMPARING THE COMPUTATIONAL COMPLEXITY OF EQUILIBRIUM PROPAGATION AND BACKPROPAGATION

324 The main motivations for using equilibrium propagation instead of an alternative machine learning technique
325 (such as deep learning using backpropagation for training) are 1) to gain insight into the operation of the
326 brain by developing target-based learning approaches in biologically plausible networks and 2) to develop
327 algorithms that are more easily implemented in hardware. Below we qualitatively compare the hardware
328 that would be needed for implementation of equilibrium propagation versus for backpropagation on a
329 standard feedforward network to gain insight into the utility of these networks.

330 ### A.1 Requirements of equilibrium propagation

Just as in the algorithm, to implement equilibrium propagation in hardware, three different phases of hardware operation are required. In the first (free) phase, it follows from equations 2, 4 and 5 that to determine its state, the i-th neuron in a network must compute

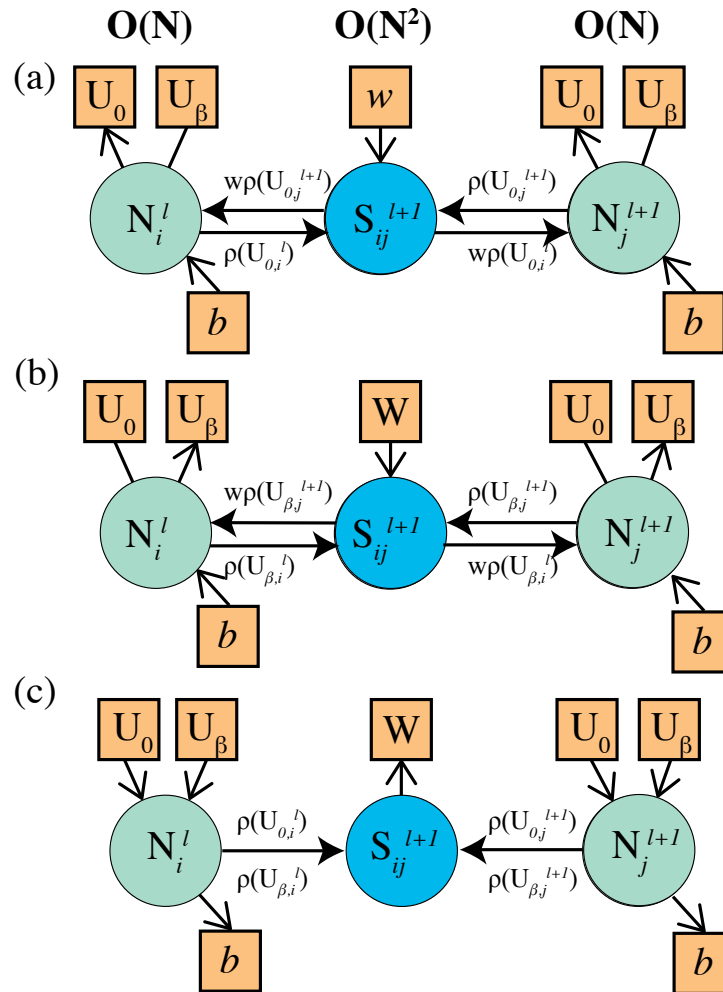$$\frac{\partial F}{\partial u_i} = u_i - \frac{1}{2}\rho'(u_i)[\sum_{i \neq j} W_{ij}\rho(u_j) + b_i],$$

Figure 6. Illustration of the functionality needed to implement equilibrium propagation in hardware. Yellow squares indicate a value that must be stored in memory for a subsequent phase. The circles indicate (N) neuron and (S) synapse devices with the associated functions described in the text. (a) The functionality required by the neurons and synapses in the free running phase. (b) The functionality of the neurons and synapses (except output neurons) in the weakly clamped phase. (c) The functionality of the neurons and synapses in the weight and bias update phase.

331 plus the term $\beta(u_i - y_i^{target})$ for output neurons when using a squared-error cost function, and then integrate
332 the result over time. Parameter correction rules are given by equations 7 and 8. This is exactly the operation
333 of an analog leaky integrate and fire neuron, as for example implemented in the neuromorphic hardware
334 platforms of references [Indiveri et al., 2011; Schemmel et al., 2010] among others. A qualitative diagram
335 of potential neuron and synapse devices and their output and read/write to memory operations are shown in
336 the diagram in figure 6 (a). At each neuron N_i^l the value of $U_{i,0}^{l+1}$ is written to memory and the nonlinear
337 function ρ is applied before sending to the synapse device, where it is multiplied by the weight w_{ij}^{l+1} which
338 is read from memory by the synapse device. These weighted outputs are summed at the input of the next
339 neuron device (N_j^{l+1}) and added to a bias value b_j^{l+1} that is read from memory to generate U_{l+1}.

340   In the second (weakly-clamped) phase, shown in figure 6 (b), the operation of the hardware is exactly
341 the same as in (a), with the value U_β written to memory at each neuron. Not shown in figure 6 is the
342 functionality at the output neurons which are weakly clamped and have a new function in this phase.
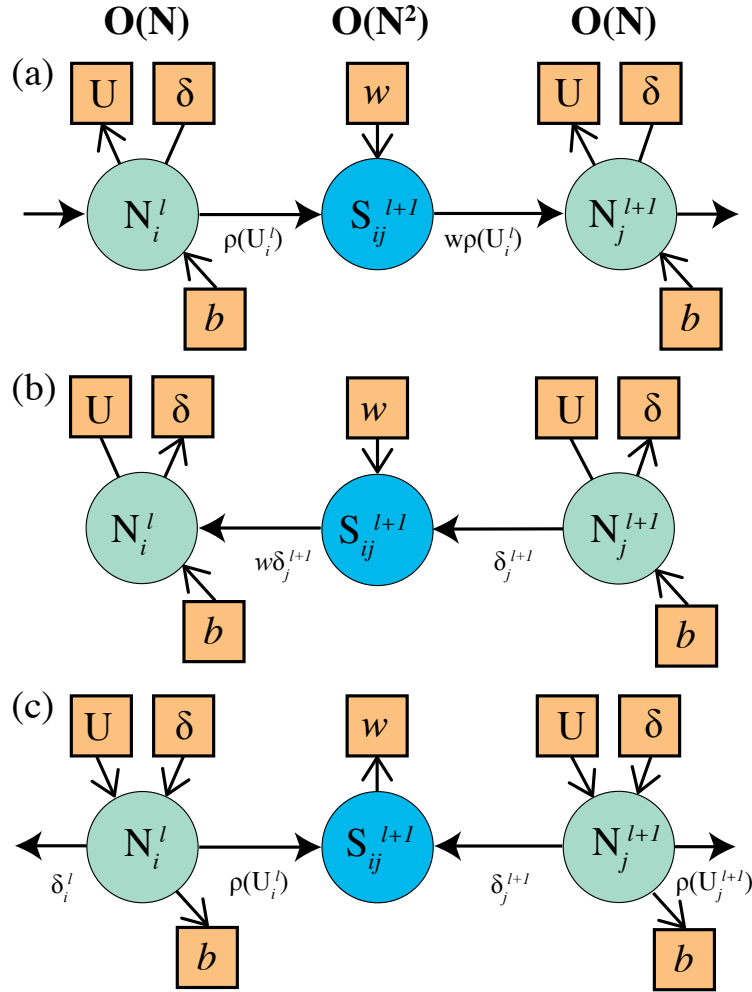
Figure 7. Illustration of the functionality needed to implement backpropagation in hardware. Yellow squares indicate a value that must be stored in memory for a subsequent phase. The circles indicate (N) neuron and (S) synapse devices with the associated functions described in the text. (a) The functionality required by the neurons and synapses in the forward pass phase. (b) The functionality of the neurons and synapses (except the last layer of neurons) in the backpropagation phase. (c) The functionality of the neurons and synapses in the weight and bias update phase.

Finally, in the third phase, the weights and biases are updated as shown in figure 6 (c). At each neuron device the values of U_0 and U_β are read from memory and $\rho(U_0)$ and $\rho(U_\beta)$ are calculated. At the synapse device, the computation of equation 7 is performed using these values from the pre- and post- synaptic neurons to calculate the weight update Δw, and the value of the weight in memory is updated to $w + \alpha \Delta w$. Similar updates are applied to the bias b at every neuron according to equation 8. As shown at the top of 6, for N such neurons per layer, there will be N^2 synapses.

A.2 Requirements of backpropagation

Backpropagation is an algorithm for training networks using gradient descent. It is most typically applied to feedforward neural networks, in which the activation value of a neuron i in layer l is given by

$$\rho(u_i^l) = \rho(\sum_j W_{ij}^l u_j^{l-1} + b_i^l).$$

This is very similar to the free running situation in equilibrium propagation, with the main difference being that the connections are unidirectional. The qualitative implementation of this inference phase in hardware is shown in Fig. 7 (a). Using backpropagation, the parameters are then updated by computing error correction terms δ_i^l for each neuron i in layer l; for the output layer L the correction is

$$\delta_i^L = \rho'(u_i^L)(\rho(u_i^L) - y_i^{target})$$

and for deeper layers it is

$$\delta_i^l = \rho'(u_i^l) \sum_j W_{ij}^{l+1} \delta_j^{l+1}.$$

The implementation of this in hardware is shown in figure 7 (b) (excluding layer L). Note that the data is now moving in the opposite (backwards) direction, and unlike in the case of equilibrium propagation, the functions implemented by the neurons are entirely different to the operation in the forward phase shown in (a). In a final phase, weights are corrected using

$$\Delta W_{ij}^l = \rho(u_i^{l-1})\delta_j^l$$

and biases using

$$\Delta b_i^l = \delta_i^l.$$

350 This is shown in figure 7 (c).

A.3 Comparison

352 The most-significant difference between the algorithms is that in equilibrium propagation, the free
353 and weakly-clamped phases of training are identical for most neurons and the weakly-clamped phase
354 requires only slight modification to output neurons, whereas in backpropagation these phases demand
355 significantly-different functionality from essentially all neurons. There are two other differences that we do
356 not believe to be significant in terms of ease of implementation in hardware. One is that in equilibrium
357 propagation each pair of neurons is joined by a bidirectional synapse, whereas in backpropagation each pair
358 is joined by two unidirectional synapses; we expect both cases to be equally easy to implement. The other is
359 that in equilibrium propagation, each neuron must remember its equilibrium state after the free phase while
360 it executes the weakly-clamped phase; since backpropagation implies a state variable for the activation and
361 error term of each neuron, the memory requirement of each neuron should be the same in both cases. For
362 a hardware implementation, the need for distinct free and weakly-clamped phases (temporally non-local
363 credit assignment) significantly reduces the advantages associated with the spatially local credit assignment.
364 Recently there has been new work that indicates that the algorithm can be modified to eliminate the need
365 for both phases [Ernoult et al., 2020]. This would significantly reduce the memory requirements of the
366 algorithm. Various characteristics of both algorithms are compared side-by-side in table 2.

FIGURES